Atmospheric
Chemistry
and Physics
Discussions

Open Access

Variability of NOx in the polar middle atmosphere from October 2003 to March 2004: vertical transport versus local production by energetic particles

M. Sinnhuber[1], B. Funke[2], T. von Clarmann[1], M. Lopez-Puertas[2], and G. P. Stiller[1]

[1]Institute for Meteorology and Climate Research, Karlsruhe Institute of Technology, P.O. Box 3640, 76021 Karlsruhe, Germany
[2]Instituto de Astrofìsica de Andalucìa, CSIC, Granada, Spain

Correspondence to: M. Sinnhuber (miriam.sinnhuber@kit.edu)

Discussion Paper | Discussion Paper | Discussion Paper | Discussion Paper

ACPD

14, 1–29, 2014

MA NOx 2003/2004

M. Sinnhuber et al.

Title Page

Abstract	Introduction
Conclusions	References
Tables	Figures

◀◀ ▶▶

◀ ▶

Back | Close

Full Screen / Esc

Printer-friendly Version

Interactive Discussion

Abstract

We use NO, NO_2 and CO from MIPAS/ENVISAT to investigate the impact of energetic particle precipitation onto the NO_x budget from the stratosphere to the lower mesosphere in the period from October 2003 to March 2004, a time of high solar and ge-

5 omagnetic activity. We find that in the winter hemisphere the indirect effect of auroral electron precipitation due to downwelling of upper mesospheric/lower thermospheric air into the stratosphere prevails. Its effect exceeds even the direct impact of the very large solar proton event in October/November 2003 by nearly one order of magnitude. Correlations of NO_x and CO show that the unprecedented high NO_x values observed

10 in the Northern Hemisphere lower mesosphere and upper stratosphere in late January and early February are fully consistent with transport from the upper mesosphere/lower thermosphere and subsequent mixing at lower altitudes; an additional source of NO_x due to local production by precipitating electrons at altitudes below 70 km as discussed in previous publications appears unlikely. In the polar summer Southern Hemisphere,

15 we observed an enhanced variability of NO and NO_2 on days with enhanced geomagnetic activity but they seem to indicate enhanced instrument noise rather than a direct increase due to electron precipitation. A direct effect of electron precipitation onto NO_x can not be ruled out, but if any, it is lower than 3 ppb in the altitude range 40–56 km and lower than 6 ppb in the altitude range 56–70 km.

1 Introduction

20

Energetic particle precipitation has been acknowledged as a source of large disturbances to the chemical composition mainly of the polar middle atmosphere for several decades. Already in the 1970s, it was recognized by Crutzen et al. (1975) and Porter et al. (1976) that precipitating energetic particles can be a source of NO_x (N, NO, NO_2)

25 in the middle atmosphere, as a result of excitation, decomposition, and ionization of the most abundant species, and due to subsequent chemical reactions of positive ions

2

with neutral species. Shortly afterwards, it was recognized that positive ion chemistry will also release active hydrogen HO_x (H, OH, HO_2) from its source, H_2O (Solomon et al., 1981). As both HO_x and NO_x destroy ozone in catalytic cycles – HO_x roughly above 45 km, NO_x below 45 km (Lary, 1997) – energetic particle precipitation events

5 are also precursors of ozone loss in the middle atmosphere.

HO_x is very short-lived throughout the middle atmosphere, and HO_x budgets will recover quickly after atmospheric ionization events. However, NO_x can be quite long-lived, depending on solar illumination – the photochemical life-time varies from hours in the sunlit middle mesosphere to days in the sunlit middle stratosphere and weeks

10 in polar night. Thus, during polar winter, NO_x produced by energetic particle precipitation can be transported down from its source regions in the polar mesosphere or lower thermosphere into the polar stratosphere, where it will then contribute to stratospheric ozone loss. This is called the "EPP indirect effect" as opposed to the "EPP direct effect" due to local production in the stratosphere and lower mesosphere (Randall et al.,

15 2007). The impact of solar proton events is nowadays reasonably well understood, in part thanks to the series of very large solar proton events during the maximum of solar cycle 23 (Jackman et al., 2001, 2005; Funke et al., 2011; Rohen et al., 2005). There is also evidence for a large indirect effect of energetic electron precipitation for many polar winters now (Randall et al., 2006, 2009; Funke et al., 2005a).

20 While effects due to large solar proton events and the indirect electron effects are reasonably well established, it is to date not clear whether there is a direct impact of energetic electron precipitation onto the stratosphere and lower mesosphere. The observational evidence gathered so far appears to be ambiguous. Callis et al. (1998) have argued for a large impact of energetic electrons onto the stratosphere based

25 on model calculations. However, no observational evidence for a direct impact below 80 km is provided by these authors. Large NO_x productions due to geomagnetic activity or relativistic electrons from the magnetosphere have been reported by Renard et al. (2006) for January 2004, by Clilverd et al. (2009) for 11–15 February 2004. However, both observations are ambigous: Funke et al. (2007) argue that the observations of

January 2004 reported by Renard et al. (2006) are equally consistent with downward transport of NO_x from the lower thermosphere, and that is more likely than direct production. Observations of MIPAS (Fischer et al., 2008) on ENVISAT considering both NO_x and the dynamical tracer CH_4 suggest that the very strong NO_x enhancement reported by Clilverd et al. (2009) in February 2004 is also more likely due to downwelling (Lopez-Puertas et al., 2006). Evidence for a possible strong impact of relativistic electrons from the radiation belt on ozone in the middle stratosphere during high winter is reported by Sinnhuber et al. (2006). However, the linking mechanism from radiation belt electrons to stratospheric ozone is not clear, as no NO_x measurements or other more direct evidence of an impact of electron precipitation at these altitudes has been presented. Verronen et al. (2011) have shown a direct impact of energetic electron precipitation on the OH abundance above 70 km altitude during two large geomagnetic storms in March 2005 and April 2006, with smaller contributions down to 50 km during one event. Sinnhuber et al. (2011) have used a long-term data-set of NO_x measurements ($NO+NO_2$) from HALOE/UARS from 1991–2005 to investigate the direct impact of energetic electron precipitation onto the middle atmosphere. Their study also shows a direct contribution from electrons mainly above 80 km, with smaller and rather sporadic contributions to lower altitudes. However, due to the poor horizontal coverage of HALOE, the results at altitudes below 80 km are not really robust. Thus it is not clear yet how large the direct impact of energetic electron precipitation on altitudes below 80 km to the overall NO_x budget is.

A more detailed summary of energetic particle precipitation onto atmospheric composition and their long-term consequences is given in the recent review by Sinnhuber et al. (2012).

We use observations of NO and NO_2 from the MIPAS instrument onboard the EN-VISAT satellite for the geomagnetically very active period from October 2003 to end of March 2004 to investigate the possible direct impact of energetic particle precipitation onto NO_x in the middle atmosphere below 70 km. CO, a tracer for air from the

4

upper mesosphere or thermosphere and for downward transport, is used to distinguish between the direct and indirect impact during polar winter.

In Sect. 2, the MIPAS data used are presented. In Sect. 3, the geomagnetic and solar activity as well as the dynamical condition of the period analysed is discussed. In Sect. 4.1, observations in the winter hemisphere, and in Sect. 4.2, observations in the summer hemisphere are discussed.

2 MIPAS data

The Michelson Interferometer for Passive Atmospheric Sounding (MIPAS) was a mid-infrared Fourier transform spectrometer observing a large number of atmospheric trace gases in limb-sounding observation mode (Fischer et al., 2008). MIPAS was launched as one of three atmospheric missions on the European Environmental Satellite EN-VISAT on 1 March 2002. ENVISAT was in a sun-synchronous orbit with an equator crossing time of 10:00 a.m. local solar time in descending mode. In 2002–2004, MIPAS sampled the atmosphere horizontally with a latitudinal spacing of $\approx 5°$ in latitude. As MIPAS measurements require no sunlight, 28 measurements are obtained in each latitude bin every day, providing a very good horizontal coverage. In the nominal measurement mode used in this study, MIPAS scans the limb tangentially from about 6 km up to 68 km.

We use NO, NO_2 and CO from MIPAS calibration version V3O derived with the level-2 IMK/IAA research processor (von Clarmann et al., 2003). Only data from version 14 is used for NO, versions 14 and 15 are used for NO_2, and versions 12 and 13 for CO. As NO2_14 and NO2_15 are very similar, as well as CO_12 and CO_13, this provides a stable, self-consistent data-set. Vertical resolution is 4–8 km for NO and NO_2 and 6–12 km for CO in the altitude range of 20–70 km. More details about MIPAS NO and NO_2 can be found, e.g., in (Funke et al., 2005b, 2011), about CO in (Funke et al., 2009).

5

Where daily averages are used, an averaging kernel criterion has been applied for NO, NO_2 and CO in such a way that only values with a mean averaging kernel larger than 0.03 have been considered. All daily averages are calculated area weighted.

3 Northern Winter 2003–2004: solar activity, geomagnetic activity, and vortex dynamics

3.1 Solar and geomagnetic activity

The time-period from first of October 2003 to end of March 2004 was chosen because it was, on the one hand, a period of very high geomagnetic activity, and on the other hand, it contained one of the largest solar particle events directly observed by particle detectors from space so far. In Fig. 1 different proxies for energetic particle precipitation for this time are shown: the Ap index as an indicator of geomagnetic activity; a merged data-set of electron fluxes from the POES instrument combinig two upward-looking channels to derive 100–300 keV precipitating electrons as described in Sinnhuber et al. (2011); and proton fluxes as measured in geostationary orbit by the particle counters onboard GOES-10. Both Ap index and proton fluxes are provided on-line from the National Geophysical Data Center NGDC (spidr.ngdc.noaa.gov/spidr).

Geomagnetic activity is high throughout the observation period, with several very pronounced intervals of enhanced geomagnetic activity lasting for many days: in mid-October 2003 before the solar proton event, in mid-November 2003, in mid-December 2003, in late January 2004, in mid-February 2004, and in mid-March 2004. These are accompanied by high fluxes of energetic electrons, especially large during several sporadic events lasting only several hours, e.g., on 15, 19, and 21, October 2003, on 11–17 and 20 November 2003, on 10–15 December 2003, on 16 and 22 January 2004, on 13 February 2004, and 2, 10, 11 and 27/28 March 2004 (marked in grey in Fig. 1). Highest electron fluxes are observed during 29 October–1 November, at the period of the solar proton event. However, during this period the electron channels

of the POES instruments are likely contaminated by high-energy protons. Solar proton events are clearly detected by enhanced proton fluxes over a large energy range from 1–100 MeV, with $\leq$ 10 MeV protons exceeding fluxes of 1 proton cm^{-2} s^{-1} sr^{-1} from 26 October to 7 November 2003. Two smaller solar proton events occur around 20–23 November and in early December 2003. During these events, proton fluxes were several orders of magnitude lower than for the October/November events, and did not exceed 10 protons cm^{-2} s^{-1} sr^{-1} for either the $\leq$ 10 MeV protons – which affect altitudes down to the lower mesosphere – or the $\leq$ 30 MeV protons – which affect altitudes down to the upper stratosphere.

3.2 Vortex dynamics

Additionally to the high geomagnetic activity, the polar winter Northern Hemisphere 2003/2004 was characterized by an interesting dynamical condition, with the occurrence of a major stratospheric warming and a vortex break-up in the upper stratosphere in late December, followed by a re-forming of the polar vortex in late January, and very strong descent which lasted well into March 2004 (Funke et al., 2009; Manney et al., 2005). A more detailed view of this winter is provided by observations of the temporal evolution of CO inside the polar vortex as shown in Fig. 2. Due to its strong vertical gradient and longevity in the polar winter vortex, carbon monoxide is commonly used as a tracer of air originating from the upper mesosphere and lower thermosphere, which is transported down into the lower mesosphere and stratosphere in the polar vortex. Enhanced values of CO are observed already in early October 2003 above 50 km, progressing steadily downward to $\approx$ 40 km until late October, signifying that a stable vortex has already formed. During November and December, downwelling of CO-rich air continues, but not as steadily as in early October, presumably due to the already enhanced wave-activity that finally led to the sudden stratospheric warming event and vortex break-up in late December. Enhanced CO volume mixing ratios (VMRs) reach about 30 km altitude in early December. In late December, the sudden stratospheric warming event starts in the upper stratosphere and mesosphere, leading to a vortex

Title Page

Abstract | Introduction

Conclusions | References

Tables | Figures

|◄ | ►|

◄ | ►

Back | Close

Full Screen / Esc

Printer-friendly Version

Interactive Discussion

break-up there. CO mixing ratios between 40–60 km altitude decrease very quickly due to mixing with mid-latitude air. Above 60 km, CO mixing ratios also decrease, but slower than in the upper stratosphere. Below 40 km, the vortex persists until January, and downwelling of CO is observed until mid-January in this altitude region. In the mesosphere above 60 km, CO mixing ratios increase again in early January, and high CO-rich air progresses downward steadily until late January, signifying the re-forming of the polar vortex and continuing downwelling in the mesosphere. However, in February and March, CO values first level off and then decrease due to the increasing contribution of photochemical loss after polar sun-rise. Thus, after late January CO is not a perfect quantitative indicator of downwelling in the polar vortex, but can still be used for identification of dynamical short-term variability in a qualitative sense.

4   Results

4.1 NO_x in the Northern Hemisphere polar vortex

The temporal evolution of NO_x ($NO+NO_2$) inside the polar vortex in Northern Hemisphere winter 2003/2004 is shown in the upper panel of Fig. 3. Three contour lines of CO are shown as well for a direct comparison between NO_x and CO (see also Fig. 2). The solar proton event on 30 October–1 November 2003 is clearly visible as a strong increase of about one order of magnitude of NO_x values within one day in the altitude range 40–70 km. Above about 60 km altitude, NO_x is already enhanced several days before the onset of the solar proton event. This might be due to downwelling in the polar vortex in early October as observed in CO observations at the same time. After the solar proton event, the behaviour of NO_x closely resembles the behaviour of CO as shown both in Fig. 2 and by the CO isolines in Fig. 3: downwelling of enhanced NO_x values in the upper stratosphere and lower mesosphere continues until the major stratospheric warming in late December, when NO_x values below 60 km altitude decrease very quickly. Above 60 km, high values of NO_x continue even after the ma-

jor warming. From mid-January on, downwelling of air very rich in NO_x is observed again. Unlike CO, stratospheric NO_x mixing ratios do not level of in late January and February, but persist to propagate downward very steadily with an average speed of $\approx 400\,m\,day^{-1}$ from the mid-mesosphere around 66 km in late January down to 45 km in mid-March (see Fig. 4). In the stratosphere, the life-time of NO_x is in the order of days to weeks even in the sun-lit atmosphere (see, e.g., Friederich et al., 2013). In the lower mesosphere above 55 km altitude, NO_x decreases during February because the NO_x life-time is in the order of a few days after polar sun-rise. While during the two periods of downwelling in October–mid-December and January–March CO mixing ratios are similar and reach values of 10–15 ppm above 60 km altitude in both periods, NO_x mixing ratios are quite different before and after the stratospheric warming event. During the strong downwelling in January and February 2004, observed NO_x mixing ratios are more than one order of magnitude higher than those produced during the solar proton event inside the polar vortex, reaching values of more than 1000 ppb in the daily average in late January and early February, compared to more than 100 ppb directly after the solar proton event.

NO_x mixing ratios of more than 1000 ppb first appear in mid-January at altitudes above 65 km, and NO_x-rich air proceeds steadily downward in the following weeks. In the following, it will be assessed whether these high amounts of NO_x are produced locally during the period of the strong geomagnetic activity in mid-January, or are due to downwelling of air from the NO maximum in the auroral zone ($\approx$ 90–120 km). Figure 5 shows daily averaged NO_x and CO altitude profiles inside the polar vortex for six days from 10 January to 2 February. Both NO_x and CO show a consistent behaviour during this time-period: an increase of the mixing ratios from 10 January to 20 January at all altitudes, and the developement of a "knee" due to photochemical loss, which is more pronounced at higher altitudes, after 20 January. The increase in volume mixing ratio (VMR) appears to be consistent with downwelling for both gases. The increase in NO_x VMRs at a given altitude is stronger than the increase in CO, because the volume mixing ratio of NO_x increases exponentially with altitude, the VMR of CO, linearly. Pho-

tochemical loss becomes evident for both NO_x and CO between 20 and 24 January, but for CO, it covers a larger vertical range: the "knee" is observed at 54 km on 2 February for CO, compared to 60–62 km for NO_x on the same day.

CO is relatively stable in the polar winter vortex; the only processes acting on local CO abundances are downward transport, mixing, and photochemical loss due to the reaction with OH. Photochemical loss of NO_x occurs with a different rate and over a different altitude regime as seen before. However, transport and mixing will act on NO_x in the same way as on CO, so the temporal evolution of the relationship between NO_x and CO can provide evidence of a direct local production of NO_x in the altitude range observed by the MIPAS NOM data, i.e., below about 70 km. A compact, non-linear relationship exists between NO_x and CO until 19 January (see left panel of Fig. 6). Non-linearity results from the different vertical gradients of NO_x and CO as seen in Fig. 5. The upper branch of the relationship with CO values $\geq$ 10 ppm and NO_x values $\geq$ 700 ppb appears only after 14 January, at altitudes above 60 km. Maximal values of more than 12 ppm CO and more than 2000 ppb NO_x are reached on 18/19 January, several days before the geomagnetic storm that peaked on 22/23 January. The very high mixing ratios of NO_x appearing first below 70 km in late January can therefore be explained by subsidence of air from the upper mesosphere or lower thermosphere, and it turns very unlikely that these very high NO_x mixing ratios are due to direct local production due to energetic particle precipitation in the vertical range covered by MIPAS NOM observations, i.e., below 70 km.

In the left panel of Fig. 6, the secant to the NO_x-CO relationship is marked as a dashed line. The region comprised by this secant and the NO_x-CO distribution (grey area) can be filled in by mixing processes. Values above this region can be gained only by direct local production of NO_x, e.g., due to energetic particle precipitation. Photochemical loss of NO_x would move the NO_x-CO pairs down, while photochemical loss of CO would move NO_x-CO pairs to the left. In the first days after 20 January 2004, the grey mixing region is indeed filled in, while later (mid to late February), the NO_x-CO pairs are moved to the left and downward. This indicates that during the time-interval

Title Page

Abstract | Introduction

Conclusions | References

Tables | Figures

◄◄ | ►►

◄ | ►

Back | Close

Full Screen / Esc

Printer-friendly Version

Interactive Discussion

from 20 January 2004 to 1 March 2004, both mixing processes and photochemical loss of NO_x and CO are important. Values above the mixing secant are not observed, so there is no evidence for a direct local production of NO_x below 70 km during this time from these observations.

In particular, there is no evidence for a strong increase of NO_x in the altitude range 50–70 km during mid-February, as discussed in Clilverd et al. (2009) based on GO-MOS observations. To investigate this in more detail, NO_x values sampled only within the geomagnetic latitudes corresponding to the radiation belts are shown in the lower panel of Fig. 3. To further exclude masking of local production by the large background values within the polar vortex, only values well outside the polar vortex (equivalent latitudes $\leq 55°$) are considered. Enhanced values of NO_x are observed above 50–60 km altitude continuosly from end of October 2003 to mid-February 2004. However, they are closely enveloped by isolines of enhanced CO values, thus are more likely remnants of vortex air than resulting from direct NO_x production. This close relationship between enhanced values of NO_x and CO throughout mid-February is also seen when looking at the spatial distribution of single observations (see Fig. 7). However, the polar vortex as indicated by high values of both NO_x and CO is elongated at the beginning of this period indicating a wave 2 pattern, which moves and expands to a more circular form from 8 February to 15 February. As the horizontal coverage of MIPAS is much better than the coverage of the star-occultation instrument GOMOS, we suggest that the apparent observation of a NO_2 enhancements on and after 11 February 2004 by GOMOS is likely due to a sampling artefact within this moving wave 2 structure.

Apart from the solar proton event in October/November 2003, no indication of direct NO_x production is observed in the MIPAS data in the Northern Hemisphere winter at altitudes below 70 km either inside or outside the polar vortex. Thus, a strong increase of NO_x due to local production by energetic electron precipitation below 70 km, as discussed e.g., by Clilverd et al. (2009), appears highly unlikely during this winter. However, it is still possible that smaller direct local NO_x production due to energetic particles occur, but are masked by the very high values observed in NO_x especially in

Title Page

Abstract | Introduction

Conclusions | References

Tables | Figures

|◄ | ►|

◄ | ►

Back | Close

Full Screen / Esc

Printer-friendly Version

Interactive Discussion

late January and February 2004. This can thus be better investigated by studying the summer hemisphere, where downwelling from the upper mesosphere or lower thermosphere does not play a role. This will be investigated in more detail in the next section.

4.2 Southern Hemisphere summer

In the Southern Hemisphere, it is polar summer in the time-period investigated. Background values of NO_x are therefore low in the upper stratosphere and lower mesosphere, and small changes can then be better discerned than in the Northern winter. However, this requires very precise observations. Because of this, NO and NO_2 will be investigated separately in the following, as NO observations in the lower mesosphere are prone to contaminations due to thermospheric cross-talk of up to 1.5 ppb. Such a cross-talk is not present in NO_2 because mesospheric and thermospheric NO_2 values are very low. NO values are sampled during day-time at solar zenith angles $\leq 88°$, NO_2 during night-time at solar zenith angles $\geq 98°$, because the partitioning of NO_x favours NO during day-time, NO_2 during night-time in this altitude range. As it is polar summer, this limits NO_2 observations to latitudes equatorwards of 64° S. To limit sampling errors, only days with more than 10 (NO_2) and 15 (NO) data-points are considered, and only data-points within 5 median absolute deviations are considered for the daily averages.

The temporal evolution of NO and NO_2 in the latitude range 52–64° S from October 2003 through March 2004 is shown in Fig. 8. NO and NO_2 show a distinct annual variability in the upper stratosphere (30–40 km) with maximal values during summer. The most distinct feature is the solar proton event in late October 2003, which leads to an increase of several tens of ppb in both NO and NO_2 above 35 km within one day. As NO_x is photochemically destroyed in the sun-lit atmosphere, it then decreases in the following days to weeks, reaching again background values in mid-November around 60 km and in mid-December around 50 km. In the latitude range chosen, 52–64° S, enhanced NO_x values do not decrease steadily. This is due at least partly to the sampling of an inhomogeneous and variable field of high values over a small (latitudinal) area.

Title Page

Abstract	Introduction
Conclusions	References
Tables	Figures

|◄ | ►|
◄ | ►

Back | Close

Full Screen / Esc

Printer-friendly Version

Interactive Discussion

If the complete polar cap is sampled, enhanced NO_x values decrease more steadily (exponentially) after the solar proton event, as shown, e.g, in Friederich et al. (2013) and in the lower left panel of Fig. 8.

Additionally to the strong enhancement of NO_x after the solar proton event in late October 2003, several enhancements with a much shorter life-time and much smaller amplitudes are observed in NO, e.g., several days before the large solar proton event on 20 October at 58–64 km, on 13 November at 58–64 km, at 18 November and 21 November at 58–62 km (see upper left panel of Fig. 8). All four days correspond to times of enhanced geomagnetic activity and increased electron precipitation on this or the previous day, see grey marks in upper left panel and Fig. 1. Apart from the very small increase on 5 December, these are also observed (with varying amplitudes) when sampling over 52–90° S, or sampling only geomagnetic latitudes corresponding to the radiation belts (see lower left and right panels of Fig. 8), so are unlikely to be due to sampling effects. The amplitudes of these enhancements are in the order of several ppb, too high to be caused by thermospheric cross-talk. However, similar enhancements are not observed in night-time NO_2 (see upper right panel of Fig. 8). This is probably due to the NO_x partitioning, which favours NO above 58 km even during night-time.

To investigate whether the observed smaller increases in NO around 58–64 km are really due to NO_x production during energetic electron precipitation events, anomalies of NO and NO_2 were calculated in the following way. For altitudes between 30–70 km, a seven-day running mean was calculated from the daily averages of NO_2 and NO (see Fig. 8) as shown exemplarily in the left panels of Fig. 9. Days with enhanced proton fluxes ($\geq 1\,\mathrm{proton\,cm^{-2}\,s^{-1}\,sr^{-1}}$ of the $\geq 30\,\mathrm{MeV}$ protons) were excluded. This corresponds to the time of the largest proton forcing during 27 October to 6 November. The weaker events in late November and early December were not excluded as proton fluxes were 3–4 orders of magnitude lower than during the October/November events. It should be noted, however, that enhanced electron fluxes and enhanced proton fluxes do not occur on the same days during these events with the exception of 22 Novem-

Title Page

Abstract | Introduction

Conclusions | References

Tables | Figures

◄◄ | ►►

◄ | ►

Back | Close

Full Screen / Esc

Printer-friendly Version

Interactive Discussion

ber, when the 100–300 keV electron flux is $\geq 2 \times 10^4$ electrons cm^{-2} s^{-1} sr^{-1}, and the 10 MeV proton flux is ≥ 2.8 protons cm^{-2} s^{-1} sr^{-1}. Anomalies are calculated as the difference of the daily average and the seven-day running mean as shown exemplarily in the right-hand panels of Fig. 9. Days with fluxes of $\geq 2 \times 10^4$ electrons cm^{-2} s^{-1} sr^{-1}

5 of the 100–300 keV precipitating electrons are marked in red. Those days are called "disturbed" in the following. The dashed blue line shows the 1 % and 99 % percentile of the distribution of anomalies, considering only days with low electron fluxes (e.g., 100–300 keV electron flux $\leq 2 \times 10^4$ electrons cm^{-2} s^{-1} sr^{-1}), derived from integration of the distribution. Positive anomalies above the 99 % percentile of the "undisturbed" days

10 are observed on several days both at 54 km and at 60 km. However, negative anomalies below the 1 % percentile also occur during "disturbed" days, suggesting that the enhanced values observed on "disturbed" days are more likely due to enhanced instrument noise rather than to an atmospheric response. Results of these investigations are summarized in the upper panel of Fig. 10. Shown are the 1 % and 99 % percentile

15 of the distribution of anomalies, considering only "undisturbed" days, compared to the highest and lowest anomalies of the "disturbed" days for altitudes from 30–70 km and for the four scenarios shown in Fig. 8. For NO$_2$, both the 98 % confidence level and the anomalies on "disturbed" days lie between −2 and 2 ppb. For NO, the 98 % confidence level lies between −2 and 2 ppb at altitudes below 56 km, but increases to 2–4 ppb

20 above depending on sampling. This indicates increased noise at higher altitudes. The maximal anomalies of the "disturbed" days behave in a similar way, increasing with altitude. Values above about 56 km are generally higher than the noise level of the "undisturbed" days, but do not show a preference for positive anomalies. This again suggests enhanced noise rather than an atmospheric response. An exception are NO

25 at 62 km in the radiation belt region, where a positive anomaly of ≈ 6 ppb is observed, and NO at 54–56 km sampled over the whole polar cap, where a positive anomaly of ≈ 3 ppb is observed. This provides an upper limit for an atmospheric response of NO$_x$ due to energetic electron precipitation: on average, it is smaller than 3 ppb below 54 km, smaller than 6 ppb between 54–70 km. However, the amplitudes of both

Title Page

Abstract | Introduction

Conclusions | References

Tables | Figures

◀ | ▶|

◀ | ▶

Back | Close

Full Screen / Esc

Printer-friendly Version

Interactive Discussion

the 98 % percentile, and of the maximal anomalies, is dominated by the period from 7 November–21 November. During this period, energetic electron fluxes were exceptionally high especially on 21 November, but there was also still a significant amount of NO_x remnant from the solar proton event. This made the derivation of a background difficult, which possibly contributes to the high observed variability. If this period is excluded from the analysis, results are qualitatively very similar, but the amplitudes are lower, less than 1.5 ppb below 54 km, and less than 3 ppb above 54 km.

5 Conclusions

– No evidence for a direct impact of energetic electron precipitation in the altitude range of the MIPAS instrument was found with the exception of the solar proton event in October/November 2003.

– Correlations of NO_x and CO show that the unprecedented high NO_x values observed in the lower mesosphere and upper stratosphere in late January and early February are fully consistent with transport from the upper mesosphere/lower thermosphere, and subsequent mixing and photochemical loss at lower altitudes. An additional source of NO_x due to local production at altitudes below 70 km as discussed in previous publications appears highly unlikely.

– Observations of NO and NO_2 anomalies in the Southern summer hemisphere suggest enhanced instrument noise during some electron events. Maximal anomalies observed give an upper limit of the impact of electron precipitation onto daily averaged NO_x at high latitudes: lower than 3 ppb in 40–56 km and lower than 6 ppb in 56–70 km.

I◄ | ►I

◄ | ►

Back | Close

Full Screen / Esc

References

Butchart, N. and Remsberg, E. E.: The area of the stratospheric polar vortex as a diagnostic for tracer transport on an isentropic surface, J. Atmos. Sci., 43, 1219–1339, 1986. 21

Callis, L. B., Natarajan, M., Lambeth, J. D., and Baker, D. N.: Solar-atmospheric coupling by electrons (SOLACE) 2. Calculated stratospheric effects of precipitating electrons, 1979–1988, J. Geophys. Res., 103, 28421–28438, 1998. 3

Clilverd, M., Seppälä, A., Rodger, C., Mlynczak, M., and Kozyra, J.: Additional stratospheric NO_x production by relativistic electron precipitation during the 2004 spring NO_x descent event, J. Geophys. Res., 114, A04305, doi:10.1029/2008JA013472, 2009. 3, 4, 11

Crutzen, P. J., Isaksen, I. S., and Reid, G. C.: Solar proton events: stratospheric sources of nitric oxide, Science, 189, 457–458, 1975. 2

Fischer, H., Birk, M., Blom, C., Carli, B., Carlotti, M., von Clarmann, T., Delbouille, L., Dudhia, A., Ehhalt, D., Endemann, M., Flaud, J. M., Gessner, R., Kleinert, A., Koopman, R., Langen, J., López-Puertas, M., Mosner, P., Nett, H., Oelhaf, H., Perron, G., Remedios, J., Ridolfi, M., Stiller, G., and Zander, R.: MIPAS: an instrument for atmospheric and climate research, Atmos. Chem. Phys., 8, 2151–2188, doi:10.5194/acp-8-2151-2008, 2008. 4, 5

Friederich, F., von Clarmann, T., Funke, B., Nieder, H., Orphal, J., Sinnhuber, M., Stiller, G. P., and Wissing, J. M.: Lifetime and production rate of NO_x in the upper stratosphere and lower mesosphere in the polar spring/summer after the solar proton event in October–November 2003, Atmos. Chem. Phys., 13, 2531–2539, doi:10.5194/acp-13-2531-2013, 2013. 9, 13

Funke, B., Lopez-Puertas, M., Gil-Lopez, S., von Clarmann, T., Stiller, G. P., Fischer, H., and Kellman, S.: Downward transport of upper atmospheric NO_x into the polar stratosphere and lower mesosphere during the Antarctic winter 2003 and Arctic winter 2002/2003, J. Geophys. Res., 112, D24308, doi:10.1029/2005JD006463, 2005a. 3

Funke, B., Lopez-Puertas, M., von Clarmann, T., Stiller, G. P., Fischer, H., Glatthor, N., Grabowski, U., Höpfner, M., Kellmann, S., Kiefer, M., Linden, A., Mengistu Tsidu, G., Milz, M., Steck, T., and Wang, D. Y.: Retrieval of stratospheric NO_x from 5.3 and 6.2 µm

nonlocal thermodynamic equilibrium emissions measured by Michelson Interferometer for Passive Atmospheric Sounding (MIPAS) on Envisat, J. Geophys. Res., 110, D09302, doi:10.1029/2004JD005225, 2005b. 5

Funke, B., Lopez-Puertas, M., Fischer, H., Stiller, G. P., von Clarmann, T., Wetzel, G., Carli, B., and Belotti, C.: Comment on "Origin of the January–April 2004 increase in stratospheric NO_2 observed in Northern polar latitudes" by Jean-Baptiste Renard et al., Geophys. Res. Lett., 34, L07813, doi:10.1029/2006GL027518, 2007. 3

Funke, B., López-Puertas, M., García-Comas, M., Stiller, G. P., von Clarmann, T., Höpfner, M., Glatthor, N., Grabowski, U., Kellmann, S., and Linden, A.: Carbon monoxide distributions from the upper troposphere to the mesosphere inferred from 4.7 µm non-local thermal equilibrium emissions measured by MIPAS on Envisat, Atmos. Chem. Phys., 9, 2387–2411, doi:10.5194/acp-9-2387-2009, 2009. 5, 7

Funke, B., Baumgaertner, A., Calisto, M., Egorova, T., Jackman, C. H., Kieser, J., Krivolutsky, A., López-Puertas, M., Marsh, D. R., Reddmann, T., Rozanov, E., Salmi, S.-M., Sinnhuber, M., Stiller, G. P., Verronen, P. T., Versick, S., von Clarmann, T., Vyushkova, T. Y., Wieters, N., and Wissing, J. M.: Composition changes after the "Halloween" solar proton event: the High Energy Particle Precipitation in the Atmosphere (HEPPA) model versus MIPAS data intercomparison study, Atmos. Chem. Phys., 11, 9089–9139, doi:10.5194/acp-11-9089-2011, 2011. 3, 5

Horne, R. B., Lam, M. M., and Green, J. C.: Energetic electron precipitation from the outer radiation belt during geomagnetic storms, Geophys. Res. Lett., 36, L19104, doi:10.1029/2009GL040236, 2009.

Jackman, C. H., McPeters, R. D., Labow, G. J., Praderas, C. J., and Fleming, E. L.: Northern Hemisphere atmospheric effects due to the July 2000 solar proton events, Geophys. Res. Lett., 28, 2883–2886, 2001. 3

Jackman, C. H., DeLand, M. T., Labow, G. J., Fleming, E. L., Weisenstein, D. K., Ko, M. K. W., Sinnhuber, M., Anderson, J., and Russell III, J. M.: The influence of the several very large solar proton events in years 2000–2003 on the neutral middle atmosphere, Adv. Space Res., 35, 445–450, 2005. 3

Jackman, C. H., Marsh, D. R., Vitt, F. M., Garcia, R. R., Randall, C. E., Fleming, E. L., and Frith, S. M.: Long-term middle atmospheric influence of very large solar proton events, J. Geophys. Res., 114, D11304, doi:10.1029/2008JD011415, 2009.

Lary, D. J.: Catalytic destruction of stratospheric ozone, J. Chem. Phys., 102, 21515–21526, 1997. 3

Lopez-Puertas, M., Funke, B., Gil-Lopez, S., von Clarmann, T., Stiller, G. P., Kellmann, S., Fischer, H., and Jackman, C. H.: Observation of NO_x enhancements and ozone depletion in the Northern and Southern Hemispheres after the October–November 2003 solar proton events, J. Geophys. Res., 110, A09S43, doi:10.1029/2005JA011050, 2005.

Lopez-Puertas, M., Funke, B., von Clarmann, T., Fischer, H., and Stiller, G. P.: The stratospheric, mesospheric NO_y in the 2002–2004 polar winters as measured by MIPAS/ENVISAT, Space Sci. Rev., 125, 403–416, 2006. 4

Manney, G. L., Krüger, K., Sabutis, J. L., Sena, S. A., and Pawson, S.: The remarkable 2003–2004 winter and other recent warm winters in the Arctic stratosphere since the late 1990s, J. Geophys. Res., 110, D04107, doi:10.1029/2004JD005367, 2005. 7

Porter, H. S., Jackman, C. H., and Green, A. E. S.: Efficiencies for production of atomic nitrogen and oxygen by relativistic proton impact in air, J. Chem. Phys., 65, 154–167, 1976. 2

Randall, C. E., Harvey, V. E., Singelton, C. S., Bernath, P. F., Boone, C. D., and Kozyra, J. U.: Enhanced NO_x in 2006 linked to strong upper stratospheric Arctic vortex, Geophys. Res. Lett., 33, L18811, doi:10.1029/2006GL027160, 2006. 3

Randall, C. E., Harvey, V. L., Singleton, C. S., Bailey, S. M., Bernath, P. F., Codrescu, M., Nakajima, H., and Russell III, J. M.: Energetic particle precipitation effects on the Southern Hemisphere stratosphere in 1992–2005, J. Geophys. Res., 112, D08308, doi:10.1029/2006JD007696, 2007. 3

Randall, C. E., Harvey, V. L., Siskind, D. E., France, J., Bernath, P. F., Boone, C. D., and Walker, K. A.: NO_x descent in the Arctic middle atmosphere in early 2009, Geophys. Res. Lett., 36, L18811, doi:10.1029/2009GL039706, 2009. 3

Renard, J.-B., Blelly, P.-L., Bourgeois, Q., Chartier, M., Goutail, F., and Orsolini, Y. J.: Origin of the January–April 2004 increase in stratospheric NO_2 observed in the Northern polar latitudes, Geophys. Res. Lett., 33, L11801, doi:10.1029/2005GL025450, 2006. 3, 4

Rohen, G. J., von Savigny, C., Sinnhuber, M., Eichmann, K.-U., Llewellyn, E. J., Kaiser, J. W., Jackman, C. H., Kallenrode, M.-B., Schroeter, J., Bovensmann, H., and Burrows, J. P.: Ozone depletion during the solar proton events of Oct./Nov. 2003 as seen by SCIAMACHY, J. Geophys. Res., 110, A09S39, doi:10.1029/2004JA010984, 2005. 3

Sinnhuber, B.-M., von der Gathen, P., Sinnhuber, M., Rex, M., König-Langlo, G., and Oltmans, S. J.: Large decadal scale changes of polar ozone suggest solar influence, Atmos. Chem. Phys., 6, 1835–1841, doi:10.5194/acp-6-1835-2006, 2006. 4

Sinnhuber, M., Kazeminejad, S., and Wissing, J. M.: Interannual variation of NO_x from the lower thermosphere to the upper stratosphere in the years 1991–2005, J. Geophys. Res., 116, A02312, doi:10.1029/2010JA015825, 2011. 4, 6

Sinnhuber, M., Nieder, H., and Wieters, N.: Energetic particle precipitation and the chemistry of the mesosphere/lower thermosphere, Surv. Geophys., 33, 1281–1334, doi:10.1007/s10712-012-9201-3, 2012. 4

Solomon, S., Rusch, D. W., Gerard, J.-C., Reid, G. C., and Crutzen, P. J.: The effect of particle precipitation events on th neutral and ion chemistry of the middle atmosphere II: odd hydrogen, Planet. Space Sci., 29, 885–892, 1981. 3

Verronen, P. T., Rodger, C. J., Clilverd, M. A., and Wang, S.: First evidence of mesospheric hydroxyl response to electron precipitation from the radiation belts, J. Geophys. Res., 116, D07307, doi:10.1029/2010JD014965, 2011. 4

von Clarmann, T., Glatthor, N., Grabowski, U., Höpfner, M., Kellmann, M., Kiefer, S., Linden, A., Mengistu Tsidu, G., Milz, M., Steck, T., Stiller, G. P., Wang, D. Y., Fischer, H., Funke, B., Gil-Lopez, S., and Lopez-Puertas, M.: Retrieval of temperature and tangent altitude pointing from limb emission spectra recorded from space by the Michelson Interferometer for Passive Atmospheric Sounding (MIPAS), J. Geophys. Res., 108, 4736, doi:10.1029/2003JD003602, 2003. 5

Title Page

Abstract | Introduction

Conclusions | References

Tables | Figures

◄◄ | ►►

◄ | ►

Back | Close

Full Screen / Esc

Title Page

Abstract | Introduction

Conclusions | References

Tables | Figures

|◄ | ►|

◄ | ►

Back | Close

Full Screen / Esc

Printer-friendly Version

Interactive Discussion
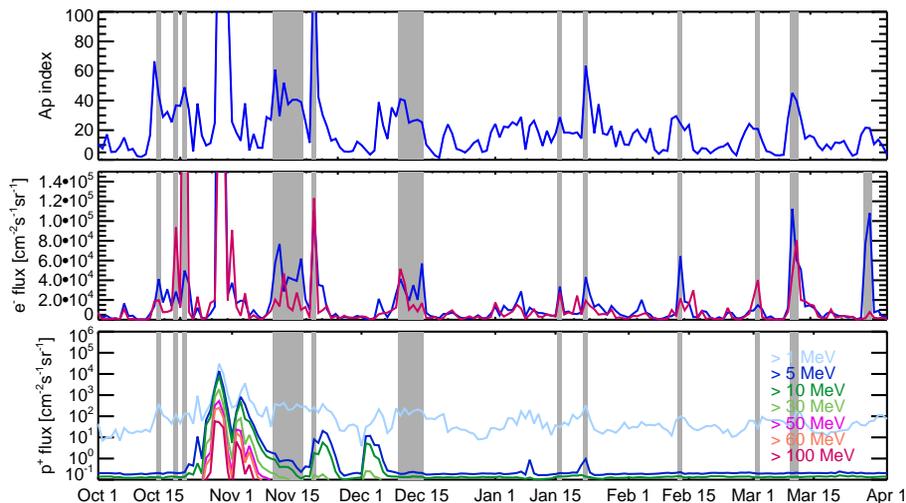
Fig. 1. Proxies for energetic particle precipitation into the atmosphere from 1 October 2003 to 30 March 2004. Top: the global Ap index as a proxy for geomagnetic activity. Middle: 100–300 keV electrons measured by the POES SEM/SEM-2 sensors in the 0° channel, which looks upward in polar regions. Red: Northern Hemisphere, blue: Southern Hemisphere. Bottom: proton fluxes at different energies measured by particle sensors on the GOES-10 satellite. Marked in grey are periods of enhanced electron fluxes, see text.
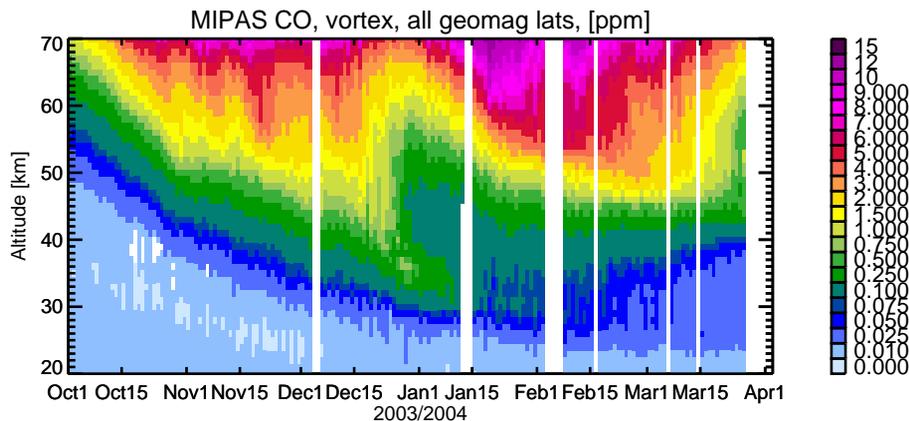
Fig. 2. CO as measured by MIPAS in the Northern Hemisphere from October 2003 to March 2004 in the latitude bin from 40–90° N, considering both day and night observations. All geomagnetic latitudes but only within the polar vortex (equivalent latitudes polewards of 65°, see Butchart and Remsberg, 1986). Only days with more than 8 data-points were used.

Title Page

Abstract   Introduction

Conclusions   References

Tables   Figures

|◄   ►|

◄   ►

Back   Close

Full Screen / Esc

Printer-friendly Version

Interactive Discussion
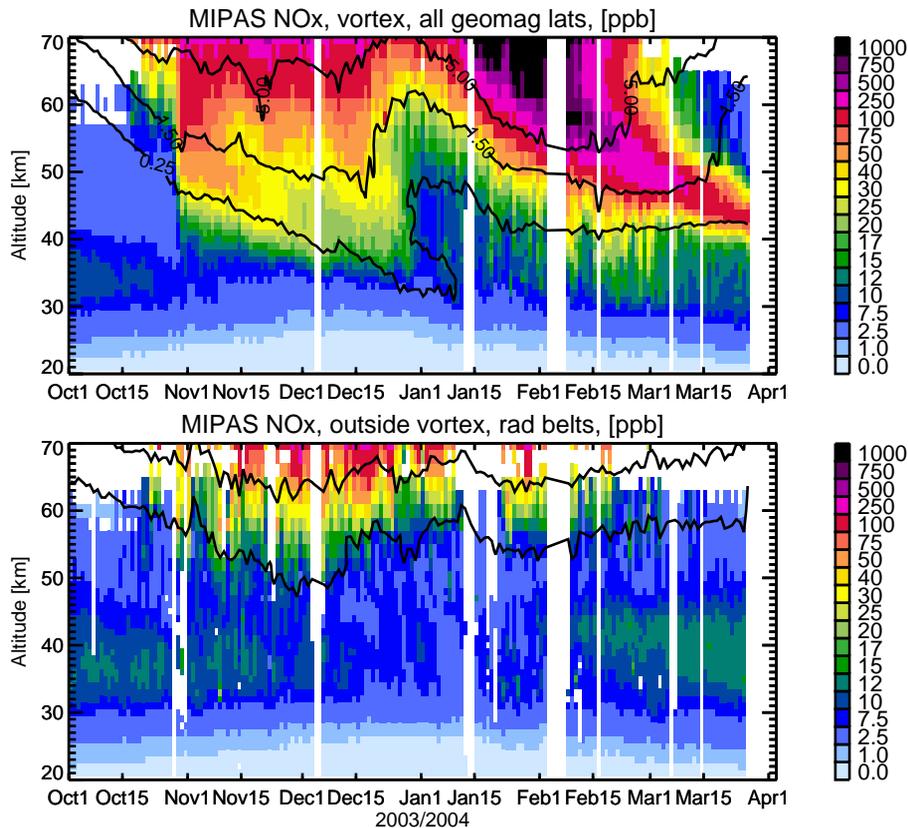
Fig. 3. Top panel: as Fig. 2, but for NO_x ($NO+NO_2$). Lower panel: as upper panel, but outside the polar vortex (equivalent latitudes $\leq 55°$), and sampled only in the radiation belt region (geomagnetic latitudes of 55–68°). Bold lines are CO isolines of 0.25, 1.5 and 5.0 ppm sampled in the same way as indicators of vertical transport and vortex origin.

Title Page

Abstract | Introduction

Conclusions | References

Tables | Figures

|◀ | ▶|

◀ | ▶

Back | Close

Full Screen / Esc

Printer-friendly Version

Interactive Discussion
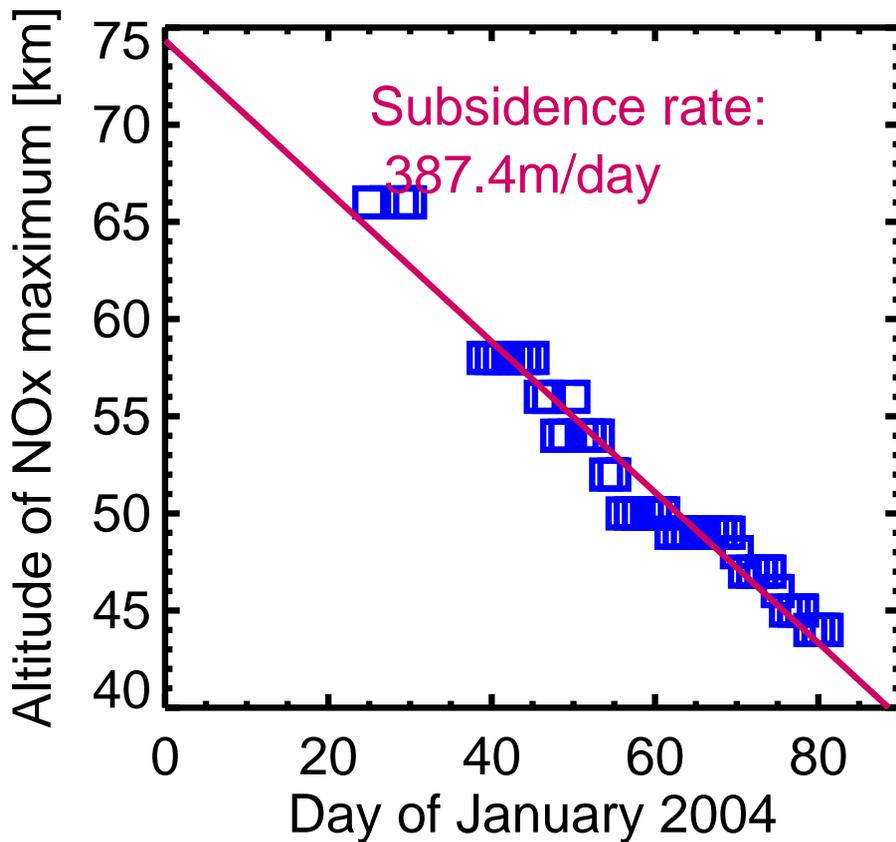
Fig. 4. Blue squares: temporal evolution of the peak altitude of NO_x as observed in MIPAS observations inside the polar vortex (equivalent latitudes polewards of $65°$ N), from January through March 2004. The red line is the result of a least-square fit to those observations, giving an average subsidence ratef of approximately $400\,\mathrm{m\,day^{-1}}$ for the NO_x maximum.

Title Page

Abstract | Introduction

Conclusions | References

Tables | Figures

|◄ | ►|

◄ | ►

Back | Close

Full Screen / Esc

Printer-friendly Version

Interactive Discussion
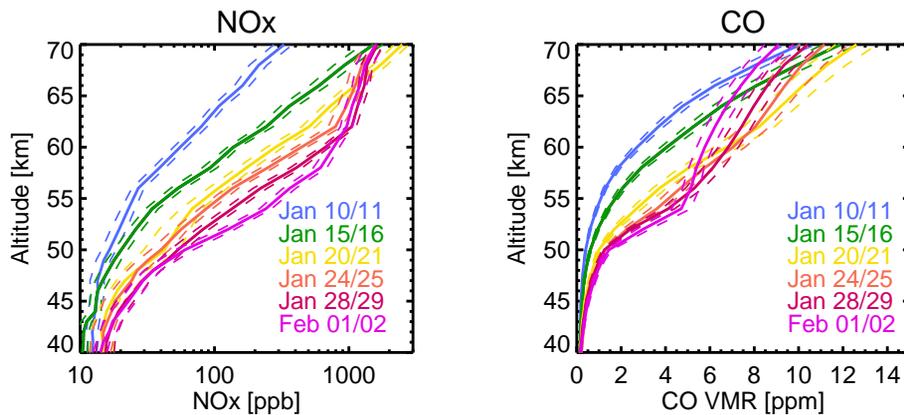
Fig. 5. Two-daily average altitude profiles of NO$_x$ (left) and CO (right) on six 2 day periods from 10 January 2004, to 2 February 2004, inside the polar vortex (equivalent latitudes poleward of 65˚). Dashed lines denote the error of the mean.
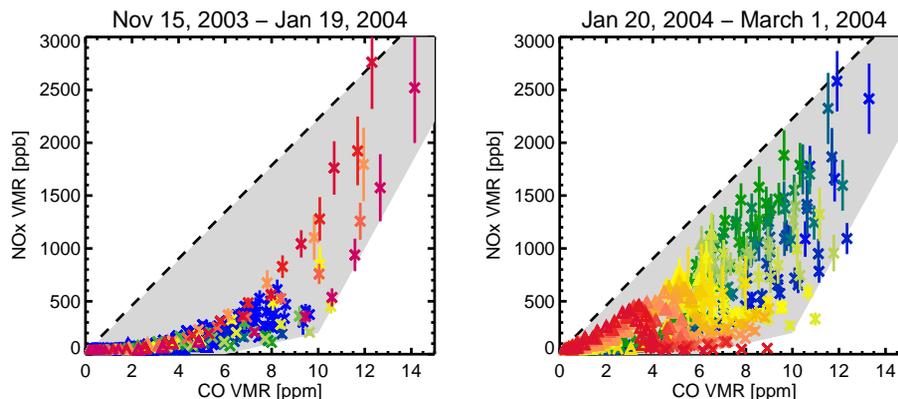
Fig. 6. Scatterplot of NOx and CO as observed by MIPAS within the polar vortex throughout NH winter 2003–2004. Left: From 15 November 2003 to 19 January 2004, considering observations in the altitude range 40–70 km. The symbols are color-coded by time, with blue denoting days in 2003, and the days in January 2004 running from green-yellow-orange-red. Dark red is 19 January. The dashed line marks the secant to this distribution, light grey marks the region incorporated by the observed distribution and its secant. Right: from 20 January to 1 March 2004. Grey area and dashed line as in left panel. Colors mark the day, running from dark blue – green – yellow – orange – red.
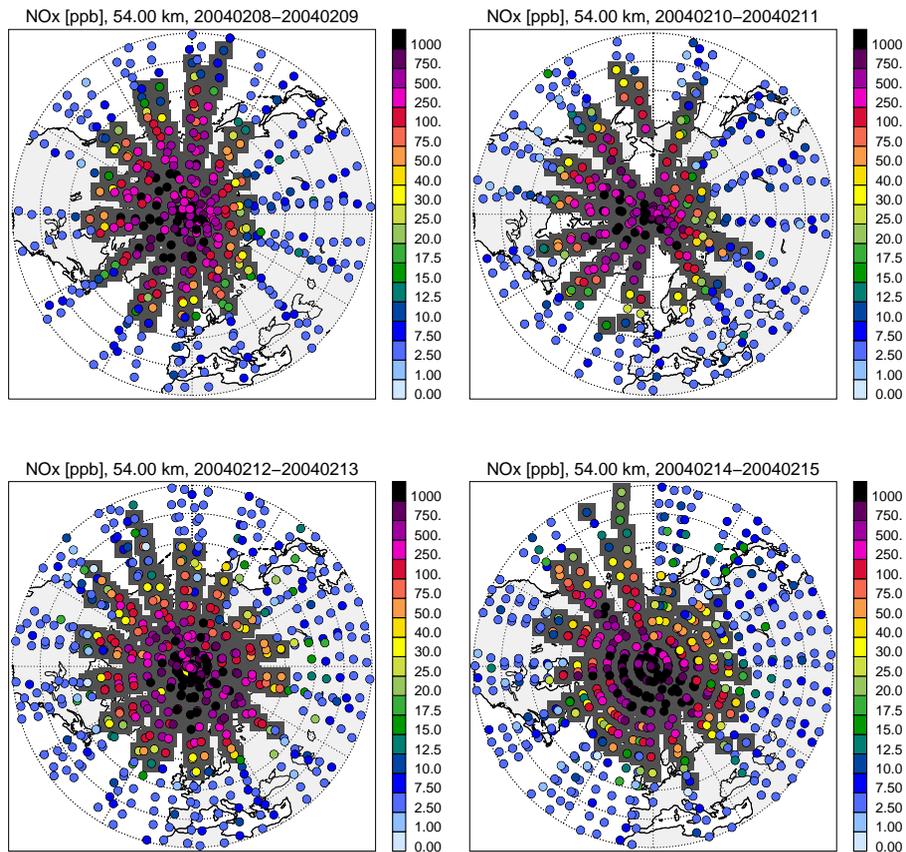
Fig. 7. NO$_x$ (day and night) single observations from MIPAS at 54 km altitude from 8 February–16 February 2004. Grey rectangles mark observations where the corresponding CO value was larger than 1 ppm marking, e.g., observations within the vortex.

Title Page

Abstract | Introduction

Conclusions | References

Tables | Figures

◄ | ►►

◄ | ►

Back | Close

Full Screen / Esc

Printer-friendly Version

Interactive Discussion
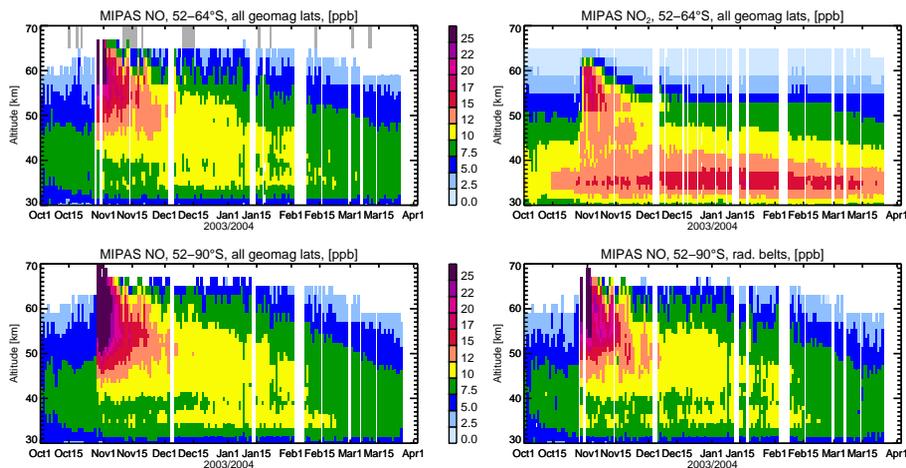
Fig. 8. Temporal evolution of day-time NO (sza ≤ 88°) and night-time NO$_2$ (sza ≥ 98°) at high Southern latitudes from 1 October 2003 to 30 March 2004. Top left: daily averages of NO from 52–64° S considering all geomagnetic latitudes. Marked in grey are days of enhanced electron fluxes, see also Fig. 1. Top right: NO$_2$ sampled over the same area. Lower panel: NO sampled over 52–90° S. Left: all geomagnetic latitudes, right: geomagnetic latitudes corresponding to the radiation belts. Only days with more than 15 data-points are considered for NO, only days with more than 10 data-points for NO$_2$, and only data-points within ± 5 median absolute deviations are considered for averaging.
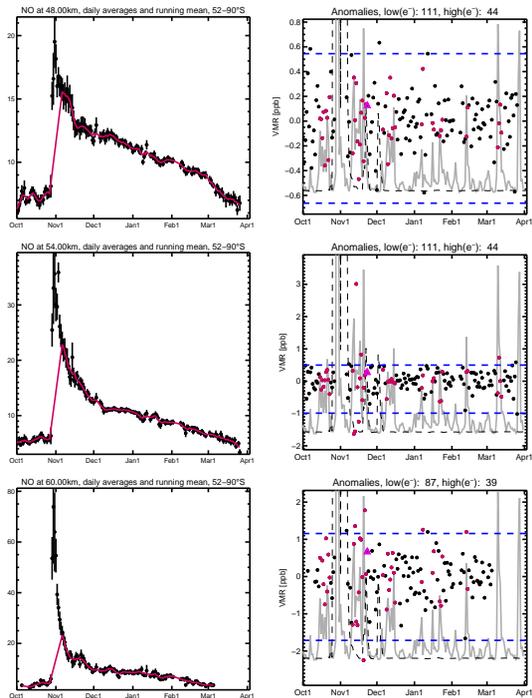
Fig. 9. Day-time NO in the latitude region 52° S–90° S at three altitudes: 48 km (upper panel), 54 km (middle panel), and 60 km (lower panel). Left panels: daily averages (black dots) and 7 day running mean (red line) excluding the period of largest proton forcing from 27 October– 6 November 2003. Right panels: anomalies (dots, daily average – running mean). Days with enhanced electron fluxes ($\geq 2 \times 10^4$ electrons cm^{-2} s^{-1} sr^{-1}) of the 100–300 keV channel on this or the previous day are marked in red. Light grey lines show the 100–300 keV electron fluxes, dashed black lines the ≥ 10 MeV proton flux for reference. Dashed blue lines mark the 1 % and 99 % percentile of the anomalies, excluding days with enhanced electron fluxes. The violett triangle marks a day with enhanced electron fluxes and ≥ 10 MeV proton fluxes.
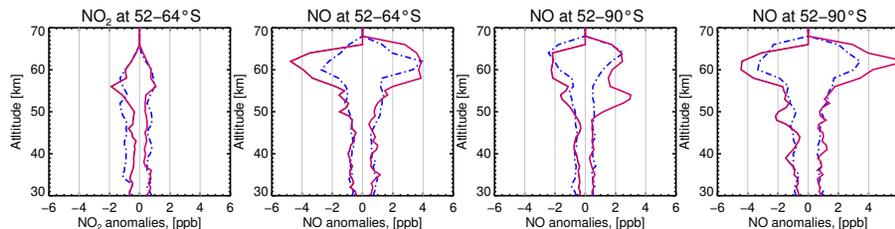
Fig. 10. Comparison of 98 % significance level for days with low electron fluxes (blue dashed lines, $\leq 2 \times 10^4$ electrons cm^{-2} s^{-1} sr^{-1} of the 100–300 keV precipitating electrons) with maximal and minimal anomalies of NO$_2$ and NO (red lines) on days of enhanced electron fluxes ($\geq 2 \times 10^4$ electrons cm^{-2} s^{-1} sr^{-1} of the 100–300 keV precipitating electrons) as a function of altitude. Outer left: Night-time NO$_2$ at 52–64° S, all geomagnetic latitudes. Middle left: day-time NO sampled over the same area. Middle right: day-time NO at 52–90° S, all geomagnetic latitudes, and outer right: day-time NO at 52–90° S, geomagnetic latitudes corresponding to the radiation belts (55–68°). The period of largest proton forcing (27 October–6 November) is excluded.

Title Page

Abstract | Introduction

Conclusions | References

Tables | Figures

|◄ | ►|

◄ | ►

Back | Close

Full Screen / Esc

Printer-friendly Version

Interactive Discussion